Electronic supplementary materials *Mendeleev Commun.*, 2026, **36**, 214–216

One-step synthesis of composite electrocatalyst of oxygen reduction reaction by electrochemical dispersion of PtCu alloy

Anastasiia V. Pugacheva, Roman A. Manzhos, Natalya S. Komarova, Aleksandr S. Kotkin, Yakov I. Korepanov, Mikhail V. Zhidkov, Evgeny N. Kabachkov, Denis V. Korchagin and Aleksandr G. Krivenko

1. Experimental

Samples for scanning electron microscopy (SEM), X-ray photoelectron spectroscopy (XPS) were prepared by drop-casting of ultra-sonicated catalyst suspension onto the surface of a conductive substrate followed by air-drying at ambient temperature. SEM images were taken with a Zeiss SUPRA 25 microscope (Carl Zeiss, Germany) equipped with an EDS detector for energy dispersive X-ray (EDX) analysis. XPS spectra were obtained using a Specs PHOIBOS 150 MCD electron spectrometer (Specs, Germany) with a Mg cathode ($h\nu$ = 1253.6 eV). The vacuum in the spectrometer chamber did not exceed 4×10^{-8} Pa. The spectra were recorded in a mode of constant transmission energy (40 eV for survey spectra and 10 eV for individual lines). The survey spectrum was recorded in 1.00 eV increments, while the spectra of individual lines were recorded in 0.03 eV increments. Background subtraction was carried out according to the Shirley method and spectra deconvolution was performed using the CasaXPS processing software (version 2.3.19). Quantification of atomic content was carried out using the sensitivity factors from the elemental library of CasaXPS. The studied area was 300–700 mm^2 while the information depth, 1–2 nm. Transmission electron microscopy (TEM) was performed on a JEM-2000FX Electron Microscope (JEOL Ltd., Japan). The samples for TEM were prepared *via* ultrasonication of the PtCu/FLGS powder in ethanol and drop-casting of the obtained suspension on a carbon-coated TEM grid. XRD pattern was recorded using an Aeris (Malvern PANalytical B.V.) XRD powder diffractometer with a Cu Kα radiation (λ = 1.5406 Å).

The linear-sweep voltammetry (LSV) measurements were performed in a three-electrode cell using a RRDE-3A ring rotating disk electrode setup (ALS Co., Ltd, Japan) with a PS-30 potentiostat (SmartStat, Russia). The glassy carbon (GC) disc 3 mm in diameter pressed in a PEEK polymer was used as a working electrode; platinum coil, as a counter electrode; and the Ag/AgCl (sat. KCl) electrode as a reference, all values of potential (E) were recalculated using the equation $E_{(\mathrm{RHE})} = E_{(\mathrm{Ag/AgCl})} + 0.198 + 0.059\mathrm{pH}$ and are given in the reversible hydrogen electrode (RHE) scale. 7 μl of the aqueous suspension of the catalyst (*ca.* 2 mg ml^{-1} for PtCu/FLGS and Pt/FLGS;

ca. 2.5 mg ml^{-1} for Pt/C) containing *ca*. 0.1 wt% of Nafion polymer were drop-cast onto the glassy carbon electrode and dried at ambient temperature. As a result, the catalyst loading was *ca*. 200 μg cm^{-2} and 250 μg cm^{-2} (Pt/C). The surface of the initial GC electrode was polished with a 0.3 μm Al_2O_3 powder. The LSV measurements were performed in O_2-saturated aqueous solution of 0.5 M H_2SO_4, potential scan rate v was 10 mV s^{-1}, electrode rotation rate was 900–4900 rpm. Kinetic currents j_k were calculated from the LSV curves using the Koutecký-Levich equation:[S1]

$$\frac{1}{j} = \frac{1}{j_k} + \frac{1}{j_d}, \qquad \text{(S1)}$$

where j_d is a density of the limiting diffusion current.

Accelerated durability test was performed as a potential cycling at a scan rate of 10 mV s^{-1} in the E region of 700–1000 V in O_2-saturated 0.5 M H_2SO_4. The LSVs for PtCu/FLGS at 2000 rpm were collected before and after 5000 potential cycles.

2. Characterization of PtCu/FLGS

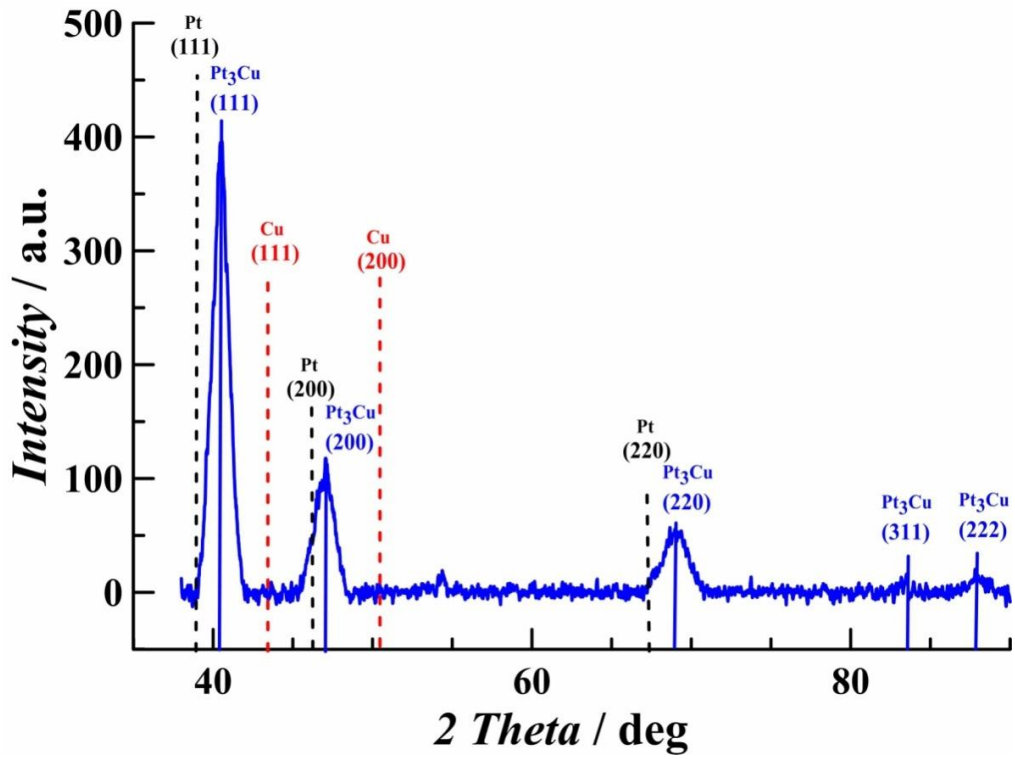

Figure S1 XRD pattern of a layer of composite PtCu/FLGS catalyst loaded onto a silicon support. Reflexes of graphite and Si support are not presented in the figure.

It is evident from the figure that only the intermetallic compound Pt_3Cu is detected (card **04-017-6718** of the Pt_3Cu compound from the PDF4 database), while free Pt and Cu as well as copper oxide are absent or their concentrations are below the detection limit of the method. This indicates that during the electrolysis synthesis, the outer Cu atoms are oxidized and replaced by

Pt, and as a result, the alloy lattice is rearranged on the surface of the nanoparticle resulting in an outer Pt layer with a minimal amount of copper. If copper oxides remain on the catalyst surface, they should be amorphous or present in a relatively small amount, since crystalline Cu phases are not detected in the diffraction patterns.[S2] An estimate of the characteristic crystallite sizes using the Scherrer formula yields a value of 4 ± 0.5 nm, which corresponds to the TEM data, see Figure 1(b).

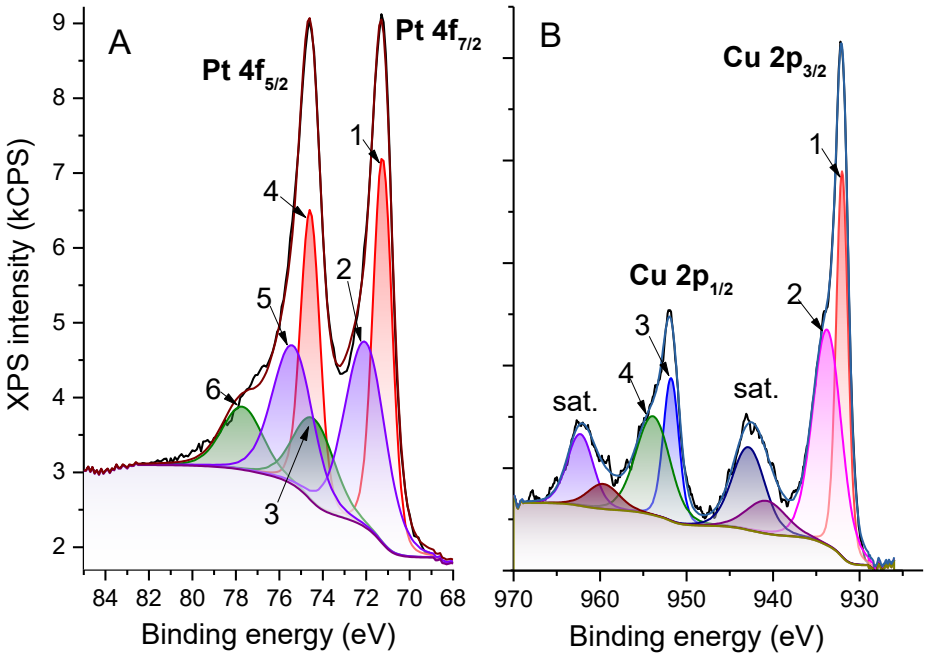

Figure S2 XPS spectra of PtCu/FLGS: (*a*) Pt 4f core level, where *1* – Pt $4f_{7/2}$ peak of metallic platinum (Pt^0), *2* – Pt $4f_{7/2}Pt(OH)_2$, *3* –Pt $4f_{7/2}$ PtO_x, *4* – Pt $4f_{5/2}$ Pt^0, *5* – Pt $4f_{5/2}Pt(OH)_2$, *6* – Pt $4f_{5/2}$ PtO_x; (*b*) Cu2p core level, where *1* – Cu $2p_{3/2}$ peak of metallic copper (Cu^0), *2* – Cu $2p_{3/2}$ CuO, *3* – Cu $2p_{1/2}$ Cu^0, *4* – Cu $2p_{1/2}$ CuO, sat. – sattelite shake-up peaks of Cu^{2+}.

Obtained experimental Pt 4f XPS spectrum of the PtCu/FLGS sample is well described by six peaks or three doublets [Figure S2(a)] corresponding to metallic platinum (Pt^0) (*1*) with E_b = 71.2 eV (Pt $4f_{7/2}$), a doublet with E_b = 72.3 eV (Pt $4f_{7/2}$) is characteristic of $Pt(OH)_2$ (*2*), and a doublet with E_b = 74.5 eV (Pt $4f_{7/2}$) indicates the presence of platinum in an oxidized state on the surface of the nanoalloy, which can be attributed to platinum oxides with the general formula of PtO_x (*3*). The spin-orbit splitting (ΔE_b) between the Pt $4f_{7/2}$ and Pt $4f_{5/2}$ levels (peaks *4*–*6*) is 3.34 eV, which is consistent with the literature data for platinum.[S3,S4] The ratio of the peak areas of the doublet components (Pt $4f_{7/2}$/Pt $4f_{5/2}$) is approximately 4:3, which corresponds to the theoretical value for these levels.

The Cu2p XPS spectrum [Figure S2(b)] contains the Cu^{2+} shake-up satellite peaks and two doublets corresponding to Cu^0 (*1*) and CuO (*2*) with E_b of 932.6 eV and 934.1 eV (Cu $2p_{3/2}$), respectively. The spin-orbit splitting between the Cu $2p_{3/2}$ and Cu $2p_{1/2}$ levels (peaks *3* and *4*) is 19.8 eV, and the ratio is 2 : 1, characteristic of Cu2p.[S5,S6]

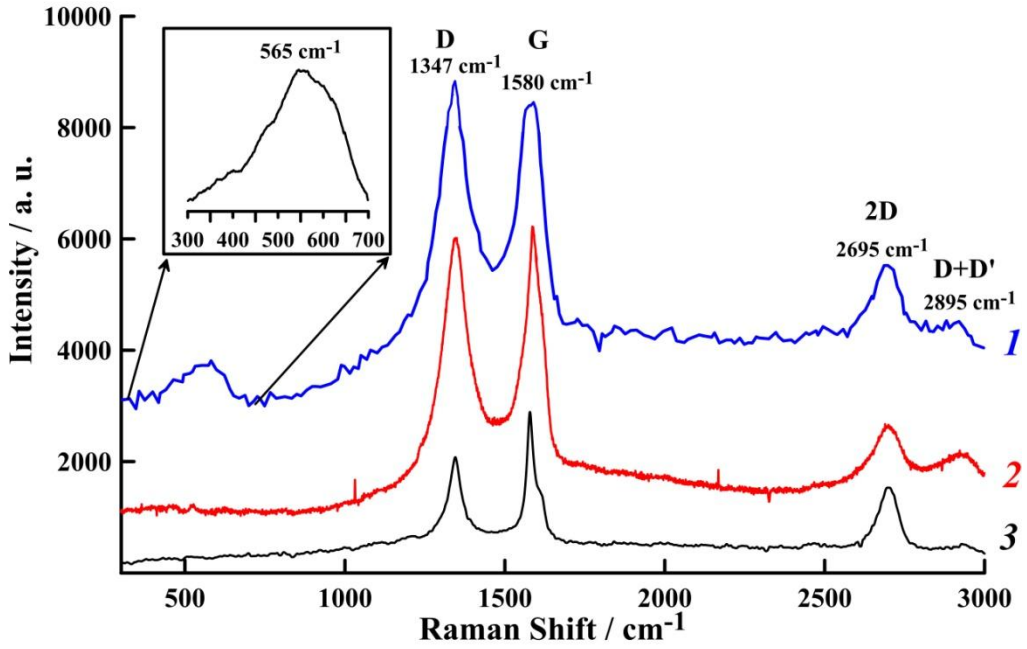

Figure S3 The Raman spectra of a layer of composite PtCu/FLGS catalyst (*1*), FLGS (*2*) and graphite (*3*) loaded onto a silicon support.

The Raman spectra of PtCu/FLGS, FLGS and graphite are presented in Figure S3. The spectra contain peaks labeled as D, G, 2D and D+D'.[S6] The bands at approximately 1580 and 2704 cm^{-1} are acceptable within the Raman selection rules and correspond to the G and 2D modes of graphene. The G mode (graphite) is associated with the tangential motion of carbon atoms and is most pronounced in graphite. The D peak (around 1350 cm^{-1}) is due to the breathing modes of sp^2 carbon atoms and is activated by defects such as boundaries, functional groups or structural disorder.[S7] It is evident from the figure that positions of D and 2D bands in the Raman spectra of the PtCu/FLGS and FLGS samples are almost identical to those for graphite, while the positions of the G bands are shifted towards higher values. The noticeable increase in the width at half maximum of D, G and 2D bands and the increase in the intensity of D band are more pronounced for PtCu/FLGS compared to FLGS. These data indicate the presence of defects on the surface of FLGS formed during the exfoliation of graphite, with the maximum number of defects observed for FLGS decorated with nanoalloy particles. In addition, unlike FLGS, the Raman spectrum of PtCu/FLGS contains a broad band at 565 cm^{-1}, which according to literature data can be attributed to the active mode of Raman scattering of monolayer platinum oxide with the general formula

PtO_x, see the inset in Figure S3.[S8] The relatively large width of the Raman band is due to the amorphous nature of the platinum surface layer.

Table S1 Halfwave potentials, kinetic currents and specific kinetic currents at 800 mV for different catalysts.

Sample	$E_{1/2}$, mV	$I_{k(800)}$, mA	$I_{k,surf(800)}$, mA cm^{-2}(Pt)	$I_{k,mass(800)}$, A g^{-1}(Pt)
Pt/FLGS	780 ± 10	–0.11 ± 0.01	–0.05 ± 0.01	–6 ± 1
PtCu/FLGS	865 ± 10	–2.24 ± 0.22	–0.72 ± 0.14	–467 ± 93[a]
Pt/C	810 ± 10	–0.55 ± 0.06	–0.15 ± 0.03	–79 ± 8

[a] in consideration that the mass fraction of platinum in the nanoalloy is *ca*. 69 % and the mass of platinum in the catalytic layer is *ca*. 4.8 μg.

References

S1 A. J. Bard and L. R. Faulkner, *Electrochemical methods: Fundamentals and applications*, 2nd edn., Wiley, New York, 2001; https://eva.fcien.udelar.edu.uy/pluginfile.php/144317/mod_resource/content/3/Electrochemical%20Methods%20Bard%20Faulkner%20Cap1-4.pdf.

S2 J. Garcia-Cardona, I. Sirés, F. Alcaide, E. Brillas, F. Centellas and P. L. Cabot, *Int. J. Hydrogen Energy*, 2020, **45**, 20582; https://doi.org/10.1016/j.ijhydene.2020.02.038.

S3 *Practical surface analysis by Auger and X-ray photoelectron spectroscopy*, eds. D. Briggs and M. P. Seah, John Wiley & Sons Ltd., Chichester, 1983, p. 533.

S4 A. Y. Lee, C. J. Powell, J. M. Gorham, A. Morey, J. H. J. Scott and R. J. Hanisch, *Data Sci. J.*, 2024, **23**, Article 45; https://doi.org/10.5334/dsj-2024-045.

S5 B. Lesiak, A. Jablonski, J. Zemek, P. Jiricek, *Surf. Interface Anal.*, 1998, **26**, 400; https://doi.org/10.1002/(SICI)1096-9918(19980501)26:5<400::AID-SIA385>3.0.CO;2-0.

S6 J. A. Torres-Ochoa, D. Cabrera-German, O. Cortazar-Martinez, M. Bravo-Sanchez, G. Gomez-Sosa and A. Herrera-Gomez, *Appl. Surf. Sci.*, 2023, **622**, 156960; https://doi.org/10.1016/j.apsusc.2023.156960.

S7 A. C. Ferrari, J. C. Meyer, V. Scardaci, C. Casiraghi, M. Lazzeri, F. Mauri, S. Piscanec, D. Jiang, K. S. Novoselov, S. Roth and A. K. Geim, *Phys. Rev. Lett.*, 2006, **97**, 51; https://doi.org/10.1103/PhysRevLett.97.187401.

S8 Y. Zhang, X. Gao and M. J. Weaver, *J. Phys. Chem.*, 1993, **97**, 8656; https://doi.org/10.1021/j100135a020.